Using acoustic emissions to enhance fracture toughness calculations for CCNBD marble specimens

K. Kaklis, S. Mavrigiannakis
School of Mineral Resources Eng., Technical Univ. of Crete, Greece
kaklis@mred.tuc.gr, smaurig@mred.tuc.gr

V. Saltas, F. Vallianatos
Dept Environmental and Natural Res. Eng., Tech. Educational Institute of Crete, Greece
vsaltas@chania.teicrete.gr, fvallian@chania.teicrete.gr

Z. Agioutantis
Department of Mining Engineering, University of Kentucky, Lexington, KY, USA
zach.agioutantis@uky.edu

ABSTRACT. Rock fracture mechanics has been widely applied to blasting, hydraulic fracturing, mechanical fragmentation, rock slope analysis, geophysics, earthquake mechanics and many other science and technology fields. Development of failure in brittle materials is associated with microcracks, which release energy in the form of elastic waves called acoustic emissions. In the present study, acoustic emission (AE) measurements were carried out during cracked chevron notched Brazilian disc (CCNBD) tests on Nestos marble specimens. The fracture toughness of different modes of loading (mode-I and –II) is calculated and the results are discussed in conjunction with the AE parameters.

KEYWORDS. Rock fracture toughness; Mode I loading; CCNBD; Acoustic emissions; Marble.

INTRODUCTION

Fracture mechanics can be applied to many engineering fields including civil and mining engineering, where drilling, excavation, explosion and cutting of rocks are closely related to the strength, stability and fracture of rock materials and structures. Fracture toughness represents the ability of a material to resist the propagation of cracks; it is considered to be an inherent property of each material and should not be related to testing conditions.

Among many different testing methods for rock fracture toughness, the International Society for Rock Mechanics (ISRM) suggests the Chevron Bend (CB) and the Short Rod (SR) specimens [1]. These tests are relevant to mode I (opening mode) fracture toughness calculations, but are not appropriate for testing the fracture toughness of rock under mode II or mixed mode I-II cases [2, 3]. Considering notched circular specimen geometries, Atkinson et al. in 1982 [4] introduced the Cracked Straight Through Brazilian Disc (CSTBD). Shetty et al., in 1985 [5], based on the CSTBD configuration, presented the Cracked Chevron Notched Brazilian Disc (CCNBD) test, by employing the straight through crack assumption. The introduction of the CSTBD and CCNBD tests, allows the determination of rock fracture toughness under mode I (opening mode), mode II (in plane shear mode) and mixed mode I-II loading cases. Both of these tests configurations show great potential for current and future applications and overcome the disadvantages of the CB and SR specimens.

The International Society for Rock Mechanics [6] suggested the cracked chevron notched Brazilian disc (CCNBD) for determining the mode I fracture toughness of rock. There are some unique features characterizing the CCNBD specimen: (a) it is closely related to the Brazilian test which is widely used for tensile strength test for rock and concrete, (b) it can be easily used for mode I, mode II and even mixed mode testing, (c) it can sustain higher critical load than other kinds of specimens with comparable size and (d) it also maintains the merit of convenience for specimen preparation from rock cores. Recent research dealt with the calibration of the minimum (critical) dimensionless stress intensity factor Y_{min}^{*} [7-9] and with measuring the fracture toughness under mode II and mixed mode I-II loading conditions using CCNBD specimens of different rock types [10, 11].

Regarding AE, it is known that a large number of such signals are generated when a rock specimen is loaded to failure. Since AE signals are caused by the formation, expansion and propagation of microcracks, such signals inherently include information related to the structural changes taking place within a rock sample.

This study focuses on the correlation between the AE signals and the diametrically applied load during CCNBD tests. The acoustic emission activity was monitored using piezoelectric acoustic emission sensors, and the potential for accurate prediction of the fracture load based on acoustic emission data is investigated.

EXPERIMENTS AND ACQUISITION OF ACOUSTIC EMISSIONS

Material

S pecimens consisting of Nestos marble were properly prepared and tested. This marble is quarried by surface mines in northern Greece and is mainly used as a building material. It is composed of 93.4% calcite, 6% dolomite and 0.6% quartz. Its density is 2.67 g/cm³ and its absorption coefficient by weight is 0.09%. It is of white color with a few thin parallel ash-green colored veins containing locally silver areas due to the existence of dolomite [12].

The geometry of the CCNBD specimen

The CCNBD specimen has the same geometry and shape (Fig. 1) as the conventional Brazilian disc used for measuring, indirectly, the tensile strength of rock. Additionally, the CCNBD specimen has a chevron notch. ISRM [6] recommends that the following dimensionless parameters can be used to characterize the geometry of the chevron notch:

$$\alpha_0 = \frac{\alpha_0}{R}, \ \alpha_1 = \frac{\alpha_1}{R}, \ \alpha_B = \frac{B}{R}, \ \alpha_s = \frac{D_s}{D}, \ \alpha^* = \frac{\alpha^*}{R} \tag{1}$$

where the diameter D is twice the radius R, B is the thickness of the disc, α_0 is the initial notch length, α_1 is the final notch length, α^* is the intermediate crack length, α_m^* is the critical crack length, and α_0, α_1, α_B, α^*, α_m^* are the relevant dimensionless expressions.

Furthermore, as shown in Fig. 1a, 2b is the crack front width, P is the load applied to the disc and D_s is the diameter of the circular cutting blade. Typical standard ratios for a CCNBD specimen suggested by ISRM [6] are given as:

$$\alpha_0 = 0.2637, \alpha_1 = 0.65, \ \alpha_B = 0.80, \ \alpha_m^* = 0.5149 \tag{2}$$

For crack lengths as presented above, high stress concentrations are generated at the crack tip which eventually lead to crack propagation and failure.

At this point it should be stressed that cracks machined by rotating cutting saws are actually of a rectangular shape thus possessing four critical points, the corners of the rectangular slit, rather than two crack tips [13]. This fact leads to a more complicated failure mechanism in the closed vicinity of the crack crown. Here however, taking also into account the AE instruments available (namely the relatively big size of sensors used), interest is focused to a wider area considering a single dominating singularity, the crack tip.
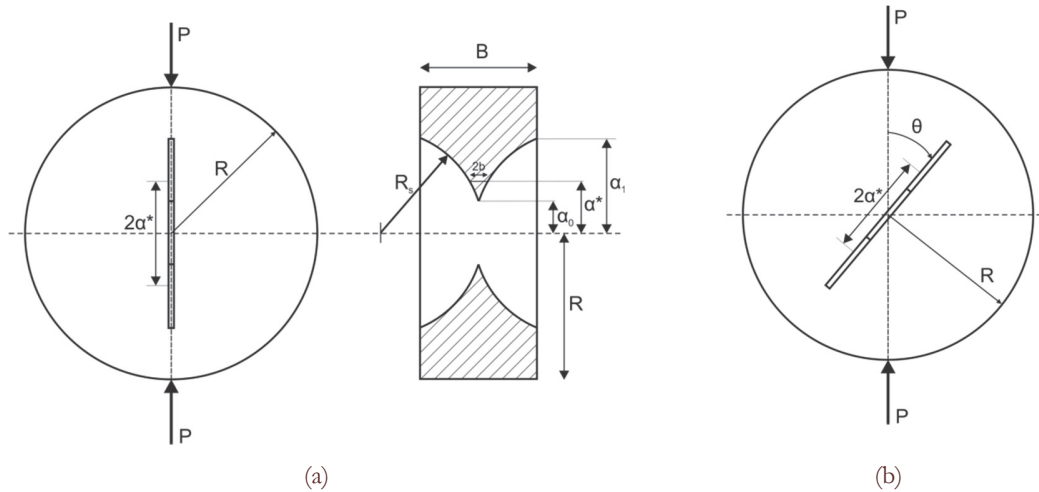

Figure 1: Geometry of CCNBD specimens under (a) pure mode I loading and (b) mixed mode I-II loading.

Fracture toughness calculation for CCNBD tests

The stress intensity factors (SIF), K_I and K_{II} for the Cracked Straight-Through Brazilian Disc (CSTBD) specimen with a through notch length of 2α, can be expressed as [5]:

$$K_I = \frac{P}{\sqrt{\pi \cdot R \cdot B}} \cdot \sqrt{\alpha} \cdot N_I \quad \text{or} \quad K_I = \frac{P}{\sqrt{\pi \cdot R \cdot B}} \cdot Y_I \tag{3a}$$

where

$$Y_I = \sqrt{\alpha} \cdot N_I \tag{3b}$$

$$K_{II} = \frac{P}{\sqrt{\pi \cdot R \cdot B}} \cdot \sqrt{\alpha} \cdot N_{II} \quad \text{or} \quad K_{II} = \frac{P}{\sqrt{\pi \cdot R \cdot B}} \cdot Y_{II} \tag{4a}$$

where

$$Y_{II} = \sqrt{\alpha} \cdot N_{II} \tag{4b}$$

where P is the load applied in compression, $a = \alpha / R$ and N_I, N_{II} are dimensionless coefficients that are functions of a and the notch inclination angle with respect to the loading direction, θ (Fig. 1b). Y_I and Y_{II} are the dimensionless stress intensity factors for CSTBD specimen.

Fig. 2 compares the geometrical terms for CSTBD and CCNBD specimens. The intermediate crack length α^* in CCNBD specimens varies between α_0 and α_1 and is regarded as equivalent of the crack length α in CSTBD specimens.
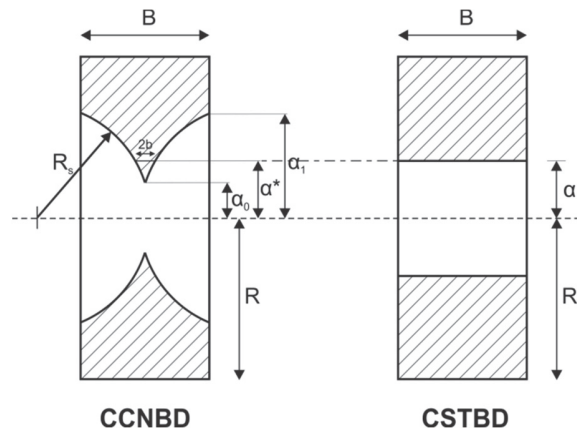
Figure 2: The geometrical definition of crack length α^* (CCNBD) and α (CSTBD).

By applying the Straight Through Crack Assumption (STCA) method [5, 14] to a CCNBD specimen, the relationships (3) and (4) take the form [10]:

$$K_I = \frac{P}{\sqrt{\pi \cdot R \cdot B}} \cdot \sqrt{\alpha^*} \cdot \sqrt{\frac{a_1 - a_0}{\alpha^* - a_0}} N_I \quad \text{or} \quad K_I = \frac{P}{\sqrt{\pi \cdot R \cdot B}} \cdot Y_I^* \tag{5a}$$

where

$$Y_I^* = \sqrt{\alpha^*} \cdot \sqrt{\frac{a_1 - a_0}{\alpha^* - a_0}} N_I \tag{5b}$$

$$K_{II} = \frac{P}{\sqrt{\pi \cdot R \cdot B}} \cdot \sqrt{\alpha^*} \cdot \sqrt{\frac{a_1 - a_0}{\alpha^* - a_0}} N_{II} \quad \text{or} \quad K_{II} = \frac{P}{\sqrt{\pi \cdot R \cdot B}} \cdot Y_{II}^* \tag{6a}$$

where

$$Y_{II}^* = \sqrt{\alpha^*} \cdot \sqrt{\frac{a_1 - a_0}{\alpha^* - a_0}} N_{II} \tag{6b}$$

where Y_I^* and Y_{II}^* are the dimensionless stress intensity factors for CCNBD specimen. Clearly, Y^* of CCNBD and Y of CSTBD are related by the following relationship:

$$Y^* = \sqrt{\frac{a_1 - a_0}{\alpha^* - a_0}} \cdot Y \tag{7}$$

The Eqs. (5) and (6) are employed to calculate fracture toughness values of CCNBD under mixed mode I-II loading. Atkinson et al. [4] provided a solution for N_I and N_{II} given by a five-term approximation (for $0.1 \leq \alpha \leq 0.6$):

$$N_I = \sum_{i=1}^{n} T_i (\alpha)^{2i-2} \cdot A_i (\theta) \tag{8}$$

$$N_{II} = 2\sin 2\theta \cdot \sum_{i=1}^{n} S_i (\alpha)^{2i-2} \cdot B_i (\theta) \tag{9}$$

where the first five values of T_i, S_i and the corresponding $A_i(\theta)$, $B_i(\theta)$ are given in Tabs. 1 and 2 in Ref. [4], respectively. Fig. 3 presents the variation of the dimensionless coefficients N_I, N_{II} with respect to the inclination angle θ for dimensionless notch lengths $\alpha = 0.1 - 0.6$.
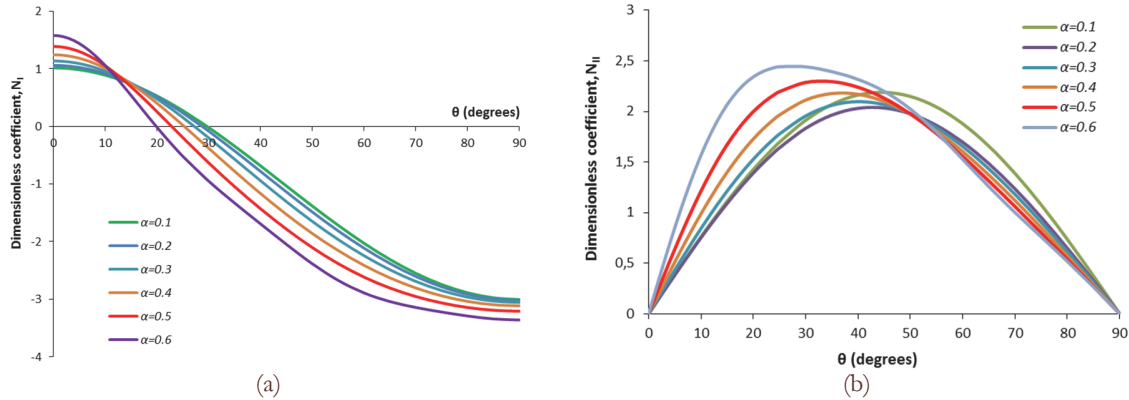

Figure 3: The dimensionless coefficients (a) N_I and (b) N_{II} for $\alpha = 0.1 - 0.6$.

In the ISRM suggested methods [6] the mode I fracture toughness K_{IC} of CCNBD specimens [6, 14, 15, 16] can be calculated by the following equation:

$$K_{IC} = \frac{P_{max}}{B \cdot \sqrt{D}} \cdot Y_{min}^* \tag{10}$$

where P_{max} is the maximum load that can be sustained by the specimen and Y_{min}^* is the minimum (critical) dimensionless stress intensity factor which is determined by the specimen geometry parameters α_0, α_1 and α_B only, and is given by:

$$Y_{min}^* = u \cdot e^{v \cdot \alpha_1} \tag{11}$$

where u and v are constants determined by α_0 and α_B only [6].

Changing the angle between loading direction and chevron notch orientation (i.e. angle θ in Fig. 1b), fracture toughness tests can be performed under mode II and mixed mode I-II loading conditions. Thus, for pure mode I loading, the crack direction should be exactly along the applied diametral force (i.e., $\theta = 0^o$), while a pure mode II condition in CCNBD specimen is achieved when the dimensionless SIF Y_I^* in relationship (5b), is equal to zero. According to Fig. 3a, $Y_I^* = 0$ when the crack inclination angle θ is about 23°. Several researchers have also determined this angle to range between 20 and 24 degrees using numerical models [11, 14]. Markides et al. [17] and Markides and Kourkoulis [18] through analytical solutions of short straight through cracks and bigger cracks obtained from elliptic holes respectively, calculated, also, this angle as a function of the dimensionless crack length from a maximum value of about 29 degrees for $\alpha / R = 0.1$ (very short crack) to about 22 degrees for $\alpha / R = 0.5$.

Calculation of the Critical crack length
Different dimensionless values for the critical crack length have been proposed in the literature. In the ISRM Suggested methods [6] it is stated that the critical crack length is $\alpha_m^* = 0.5149$ (for a specimen geometry given by Eq. (2)) without any explanation of how this value was calculated. For the exact same specimen geometry, Wang et al. [7] proposed to use a critical crack length of 0.49, while a value of 0.4915 is derived in the present paper, by minimizing the dimensionless Stress

Intensity Factor Y^*. More specifically, the upper curve shown in Fig. 4 represents the dimensionless stress intensity factor of the CCNBD specimen for various crack lengths as obtained from Eq. (5b) in conjunction with Eq. (8) for mode I, while the lower curve corresponds to the dimensionless SIF of the CSTBD specimen as obtained from Eq. (3b) in conjunction with Eq. (8) also for mode I. It is observed that the SIF for the CSTBD specimen monotonically ascends, while the SIF curve for the CCNBD specimen is convex and reaches a minimum value between the initial and final crack length. The minimum SIF value for the CCNBD specimen $Y^*_{min} = 1.2578$ corresponds to the critical crack length $\alpha^*_m = 0.4915$. When $\alpha^* \geq \alpha_1$, it is assumed that the SIF for the CCNBD specimen is identical to that of the CSTBD specimen as discussed by [7] and [9].
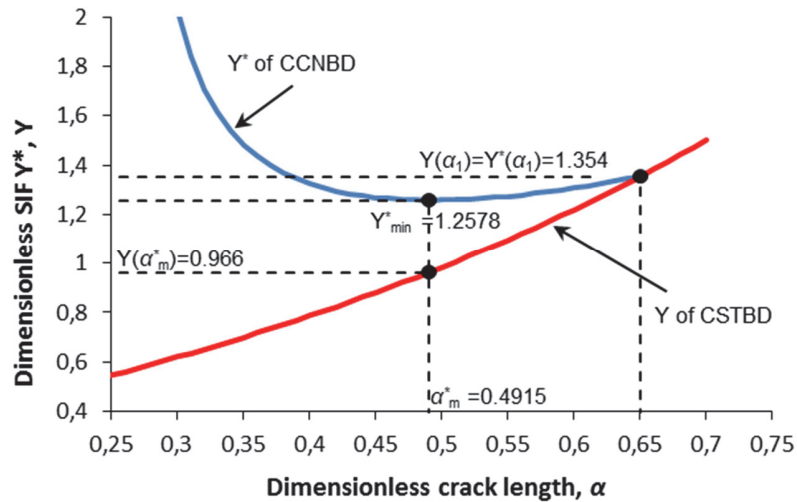

Figure 4: Dimensionless stress intensity factors for straight through and chevron notches in a CCNBD specimen with $\alpha_0 = 0.2637$ and $\alpha_1 = 0.65$.

Specimen preparation and experimental setup
Initially, the circular discs of Nestos marble (D = 52 mm) were prepared by coring specimens out of Nestos cubes with their long axis normal to the plane of transverse isotropy (Fig. 5), in order to avoid large variations in the quality of the stone and ensure similar fracture loads.
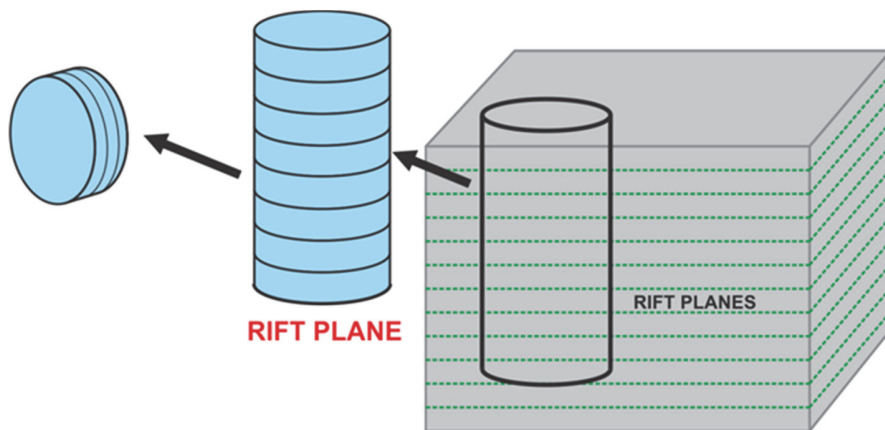

Figure 5: Specimen orientation. The middle plane of the disks is parallel to the plane of transverse isotropy (rift planes).

The CCNBD specimens were prepared according to the standard geometrical dimensionless expressions (2) [6]. Two chevron notches (one in each side) were cut in the center of each disc by using a thin rotary diamond saw with a diameter of D_s = 38 mm and a thickness of t = 1 mm which results in a crack width of less than 1.5 mm (Fig. 6). This satisfies the requirements suggested by [6,9,10,14] that the machined crack width should not exceed 1.5 mm. Wang et al [19]

emphasize that the notch width has an important effect on the stress intensity factors and that the crack width should be adequate to ensure crack propagation. At the same time Shetty et al. [5] indicate that they used a machined slot opening of 250 μm without giving any technical details. The indentation depth of the rotary saw on each side of the disc was about 11.72 mm and thus, two V shape chevron notches were introduced in the circular disc. The diamond saw was cooled by water during the chevron notch cutting process.
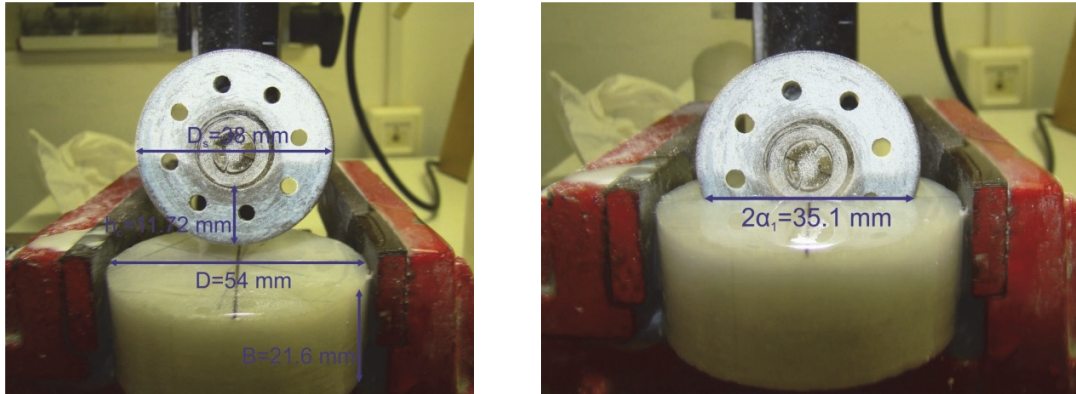

Figure 6: The schematic cutting configuration for preparing CCNBD specimens with some theoretical geometrical parameters.

Fig. 7a presents the final configuration of a CCNBD specimen with the theoretical dimensional parameters α_0 and α_1. In order to obtain consistent test results and to satisfy the plane strain condition, the ISRM [6] prescribes that the range of α_1 and α_B is restricted as shown in Fig. 7b. It is evident that the selected geometric parameters (2) are located within the valid range.
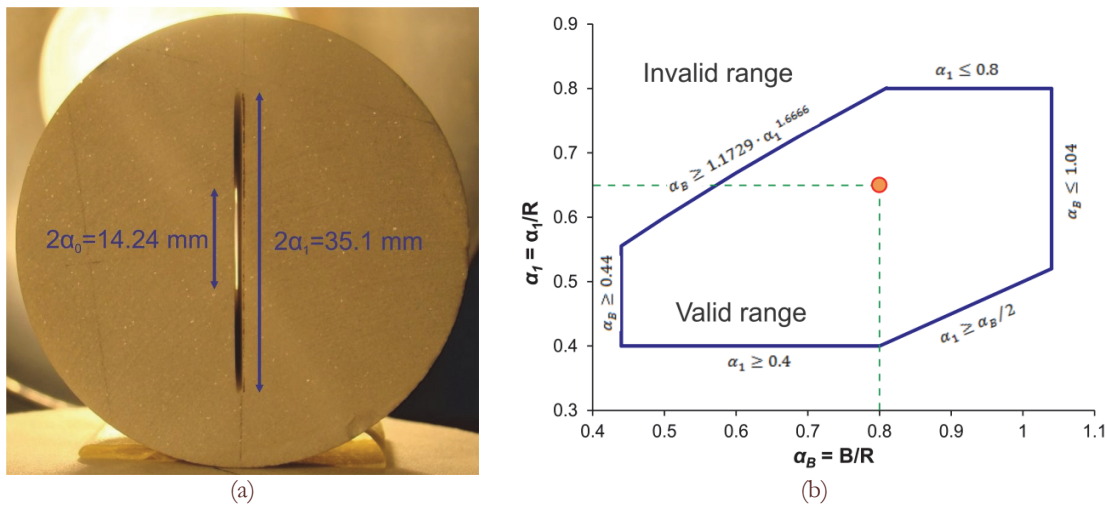

Figure 7: (a) CCNBD specimen. (b) The valid geometrical range for CCNBD specimen.

The CCNBD specimens (Fig. 7a) were then placed in the Brazilian testing apparatus and loaded by a diametral compressive force P. For pure mode I loading, the crack direction should be exactly along the loading diameter, while for mixed mode I-II loading the chevron notch orientation lies between 0 and 90 degrees. Load was applied using a stiff 1600 kN MTS hydraulic testing machine and a 500 kN load cell, with a loading rate of 200 N/s under load control mode for all experiments.

Monitoring of Acoustic Emissions
The AE activity may be represented in time series of detected signals in each sensor (hits), their amplitudes (signal peak in dB), rise time (RT) which is defined as the time between the first threshold crossing (FTC) and the point of peak amplitude, as well as other acoustic parameters. AE signals were acquired and analyzed using the AE WIN software

package by Enviroacoustics [20]. Acoustic emission signals were detected through 6-8 miniature piezoelectric sensors (PICO sensors, 200 kHz-1 MHz, MISTRAS Group, SA) mounted on the surface of each specimen and recorded through an integrated multi-channel system of Physical Acoustics Corporation. The positions of the sensors on each side of the CCNBD specimens for the determination of the mode I ($\theta=0^o$) and mode II ($\theta=23^o$) fracture toughness are shown in Fig. 8 and Fig. 9, respectively. Usage of such sensors was dictated due to the small size of the specimens. Their high sensitivity over a broad bandwidth ensures the accurate detection of the AE signals. It should be noted that in the case of the specimens subjected to mode I loading, the positions of the AE sensors were symmetrically located with respect to the tips, while in the case of the mode II loading the positions were somewhat arbitrary positioned on the surface of the specimens. In both cases, however, the accurate determination of the events' location is mainly limited by the size of the sensors and to a lesser extent by their positions, as discussed in the next section.

The source location of the AE events on a planar projection was determined by using the arrival times of the hits detected by at least three sensors. This procedure is described in details elsewhere [21].
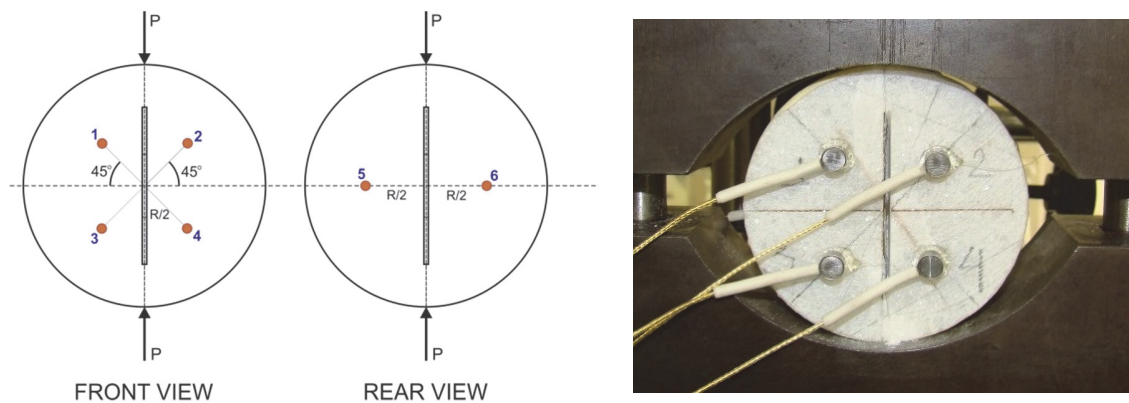

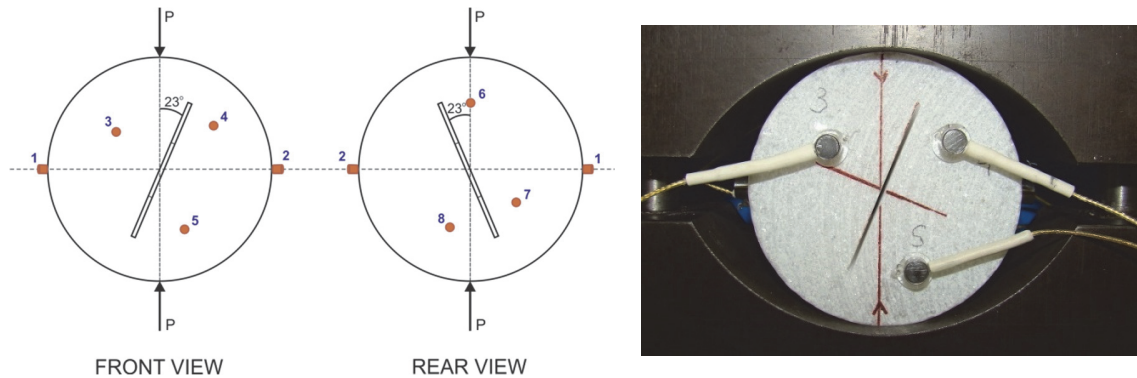Figure 8: The positions of the sensors for the mode I ($\theta=0^o$) loading CCNBD specimens.

Figure 9: The positions of the sensors for the mode II ($\theta=23^o$) loading CCNBD specimens.

EXPERIMENTAL RESULTS ANS DISCUSSION

Rock fracture toughness for pure mode I

Six CCNBD tests were performed for the determination of mode I fracture toughness (Fig 8). The fracture load was identified using AE records and the specimen fracture toughness was calculated using Eq. (10). The average fracture toughness of these specimens was (0.73 ± 0.08) MPa m$^{1/2}$ (Tab. 1).

The minimum dimensionless stress intensity factor Y^*_{min}, is an important calculation parameter which greatly affects the accuracy of toughness tests. It is calculated using Eq. (11) and the values of parameters u, v, as suggested by the ISRM [6]. In order to improve the fracture toughness tests using CCNBD, recent research [8, 9, 16], based on the slice synthesis method [22] and other numerical methods, presented updated values of the two parameters of the exponential function (Eq. (11)) that cover a wide range of specimen geometries.

Tab. 2 presents the rock fracture toughness calculated by Eq. (11) using parameter values u and v from the original tables of the ISRM [6] and three other publications. It is noteworthy that the difference between the average fracture toughness calculated by the ISRM and the three other publications is about 12%. Note that the K_{IC} values presented in Tab. 2, are calculated using the u and v values proposed by ISRM [6] and those proposed by other researchers [8, 16, 9], while the K_{IC} value for [5] is calculated using $\alpha_m^* = 0.4915$.

Specimen	Thickness (mm)	Diameter (mm)	α_0	Fracture load (kN)	Y_{min}^* [6]	K_{IC} $\left(MPa \cdot m^{1/2}\right)$
2.1	21.00	52.30	0.229	4.35	0.83	0.75
2.2	20.75	52.20	0.234	3.63	0.83	0.64
2.3	20.75	52.20	0.241	4.33	0.83	0.76
3.3	20.80	52.17	0.230	3.72	0.83	0.65
4.2	20.75	52.17	0.264	4.95	0.84	0.88
4.3	20.50	52.23	0.302	3.81	0.85	0.69
Average				4.13	0.83	0.73
St. Dev.				0.46	0.01	0.08

Table 1: Geometrical parameters, fracture loads and fracture toughness of CCNBD specimens under pure mode I loading (the value for Y_{min}^* was calculated based on eq. (11) using the values for u and v given by ISRM [6] in table form).

Specimen	ISRM [6]	Wang et al. [8]	Wang [16]	Wang et al. [9]	Shetty et al. [5]
2.1	0.75	0.85	0.84	0.86	0.91
2.2	0.64	0.72	0.72	0.73	0.77
2.3	0.76	0.86	0.85	0.87	0.91
3.3	0.65	0.73	0.73	0.75	0.78
4.2	0.88	0.99	0.99	1.00	1.05
4.3	0.69	0.78	0.78	0.80	0.81
Average	0.73	0.82	0.82	0.84	0.87
St. Dev.	0.08	0.10	0.10	0.10	0.10

Table 2: Comparison of rock fracture toughness $K_{IC} \left(MPa \cdot m^{1/2}\right)$ for the CCNBD specimens.
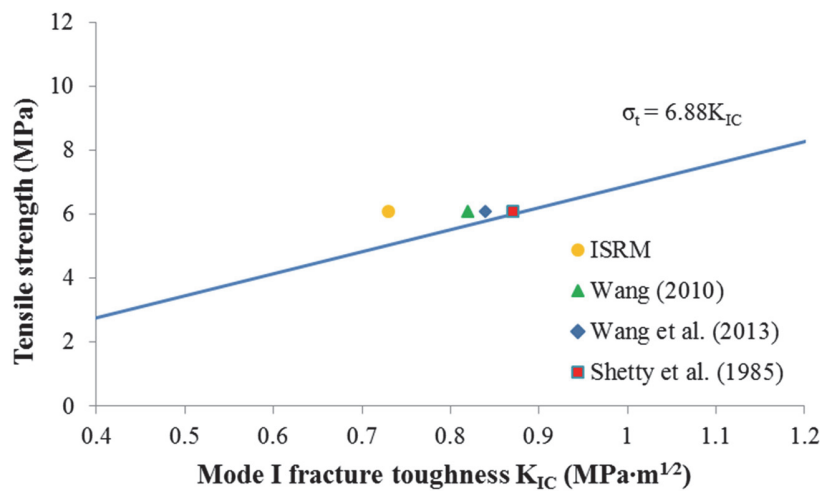

Figure 10: Correlation between the tensile strength and mode I fracture toughness based on different methodologies.

Furthermore, Zhang [23] correlates the mode I fracture toughness and tensile strength of different rock types through the following equation:

$$\sigma_t = 6.88 \cdot K_{IC} \qquad\qquad (12)$$

For comparison, the average values of mode I fracture toughness obtained for Nestos marble as shown in Tab. 2 were plotted together with Eq. (12). A tensile strength for the Nestos Marble equal to 6.07 MPa (determined experimentally using a traditional Brazilian test) was used for all data points. Experimental results correlate well with the values generated by Eq. (12) except for the value obtained via the ISRM (Fig 10).

Rock fracture toughness for pure mode II

The orientation of the chevron notch crack of the CCNBD specimen, for the determination of the fracture toughness for pure mode II loading was $\theta = 23°$ from the loading direction. The fracture toughness K_{IIC} values were calculated using Eq. (6a) with the aid of relationship (9) (Tab. 3). Two sets of K_{IIC} values are provided in Tab. 3, calculated for different critical crack lengths. In the first case, K_{IIC} was calculated using a critical crack length calculated by minimizing Y^*_{min} while in the second case the critical crack length was set equal to 0.36 [10].

Specimen	Thickness (mm)	Diameter (mm)	α_0	α_1	Fracture load (kN)	N_{II}	K_{IIC} $\left(MPa \cdot m^{1/2}\right)$ $\left(a^*_m = 0.4915\right)$	K_{IIC} $\left(MPa \cdot m^{1/2}\right)$ $\left(a^*_m = 0.36\right)$
CCNBD 1	20.90	52.30	0.262	0.679	5.10		1.64	1.84
CCNBD 2	20.85	52.35	0.263	0.685	4.89		1.58	1.77
CCNBD 3	21.20	52.30	0.229	0.672	5.90		1.87	2.10
CCNBD 6	21.25	52.25	0.270	0.684	5.98	1.8013	1.89	2.13
CCNBD 7	19.50	52.30	0.350	0.677	4.73		1.63	1.83
CCNBD 8	21.00	52.30	0.281	0.673	4.89		1.57	1.76
CCNBD 9	21.60	52.30	0.242	0.675	4.95		1.54	1.73
Average					5.21		1.67	1.88
St. Dev.					0.51		0.15	0.16

Table 3: Geometrical parameters, fracture loads and fracture toughness of CCNBD specimens under pure mode II loading.

Crack growth and mode of fracture

The crack growth for mode I specimens was along the chevron notch plane and the tensile splitting was the dominant failure mode. Fig. 11 shows a typical CCNBD specimen fractured under pure mode I loading. For mode II loading where the angle between the applied stress and the chevron node direction is 23°, a typical fractured specimen is illustrated in Fig. 12.
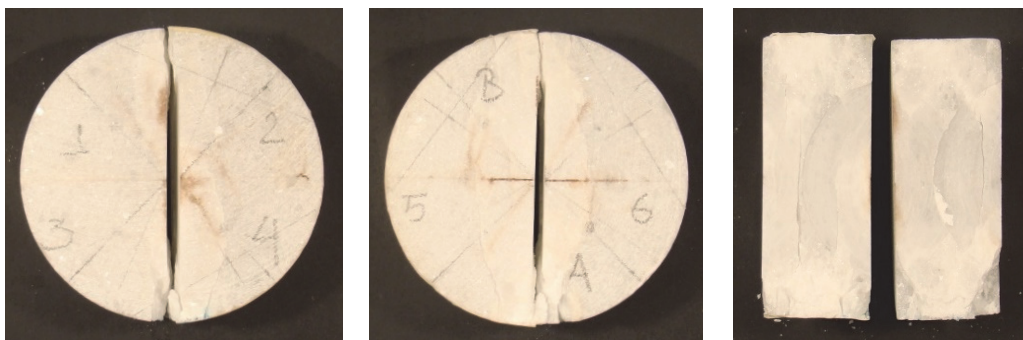

Figure 11: A typical CCNBD specimen fractured under mode I loading.

Figure 12: A typical CCNBD specimen fractured under mode II loading.

At this point it should be mentioned that investigation of the closed vicinity of the 'crack tip', particularly in the case of mode-II loading, reveals that crack growth seems to start from the inner edge of the chevron slit and then propagates towards the corner points of the slit that are nearer to the points of application of the externally applied load (Fig 12).That seems to be the case even for mode-I loading (Fig.11), due, however, to reasonable imperfections detected in the final shape of the chevron slit.

That phenomenon may, in a first approximation, be attributed to the fact that the corner points nearer to the points of application of the externally applied load are under a combined tensile and shearing stress field probably enhancing fracture, while the opposite ones are under a combined compressive and shearing stress field [13], probably not enchasing fracture.

In this context, the SIF concept referring to mathematical cracks, should be considered with extra care, when it comes to slits.

In addition, it should also be mentioned that the fracture patterns detected in the vicinity of the disc-jaw contact region (visible at the bottom areas of contact in Figs. 11, 12) and the possibility of premature fracture in these areas (even in the present case of the pre-CCNBD specimen), are probably attributed to frictional stresses developed at the contact areas to counterbalance the rotation tendency of the disc as a whole due to the presence of the slope slit [24]. This may be an area to be closely monitored in subsequent experiments by potentially using additional piezoelectric sensors at these regions of the specimen.

Acoustic emission results

The time evolution of various acoustic emission parameters during the CCNBD test of a representative specimen (specimen 2.3) subjected to mode I fracture (see Fig. 11) is shown in Fig. 13a-d. Observable AE activity starts at the time t=30 s of the test, i.e., just before the occurrence of the first macroscopic crack at the load of 4.3 kN. The final rupture of the specimen occurs at around 54 s, as it is evident from the corresponding drop in the load which is also accompanied with relatively high amplitudes of the recorded signals in all channels (see Fig. 13a).

It is noteworthy that the first macro-crack is clearly distinguished in the recorded parameters since it is associated with an abrupt increase of recorded hits with high amplitudes (see Fig. 13a, c) and the corresponding observed peak of high hit rate at around 33 s (see Fig. 13b). In contrast, the recorded relatively high mean hit rate and the corresponding uniform increase of cumulative hits after 52 s are not sufficient to correlate them with the final rupture of the specimen. An important AE parameter which has also to be considered is the rise time (RT) of the recorded waveforms that gives us information about the fracture process [25]. It is evident from Fig. 13d that high values of RT are observed at around t = 32.5 s due to the formation of the first macroscopic crack and afterwards during the stage of the final rupture (53 - 54 s). In the intermediate region, the mean value of RT remains almost constant (RT < 250 µs), while the AE activity increases continuously. These low values of RT are related to the formation of tensile micro-cracks while, the high recorded values are due to the formation of mixed mode cracks (tensile and shear) observed either solely during the formation of the macroscopic crack at the initial stage of loading (around 32.5 s), or at the final stage where the coalescence of the existent cracks takes place, leading to the ultimate rupture of the specimen [25]. Notably, during the final rupture of the specimen (at 53-54 s), the load does not decrease abruptly as it could be expected, while, large values of amplitudes are still observed afterwards. This is attributed to the fact that although the specimen was separated into two parts (see Fig. 11), it retained its stability, while considerable AE activity is produced due to the friction between, either the two separated parts of the fractured specimen, or the mounting jaws and the surface of the specimen.
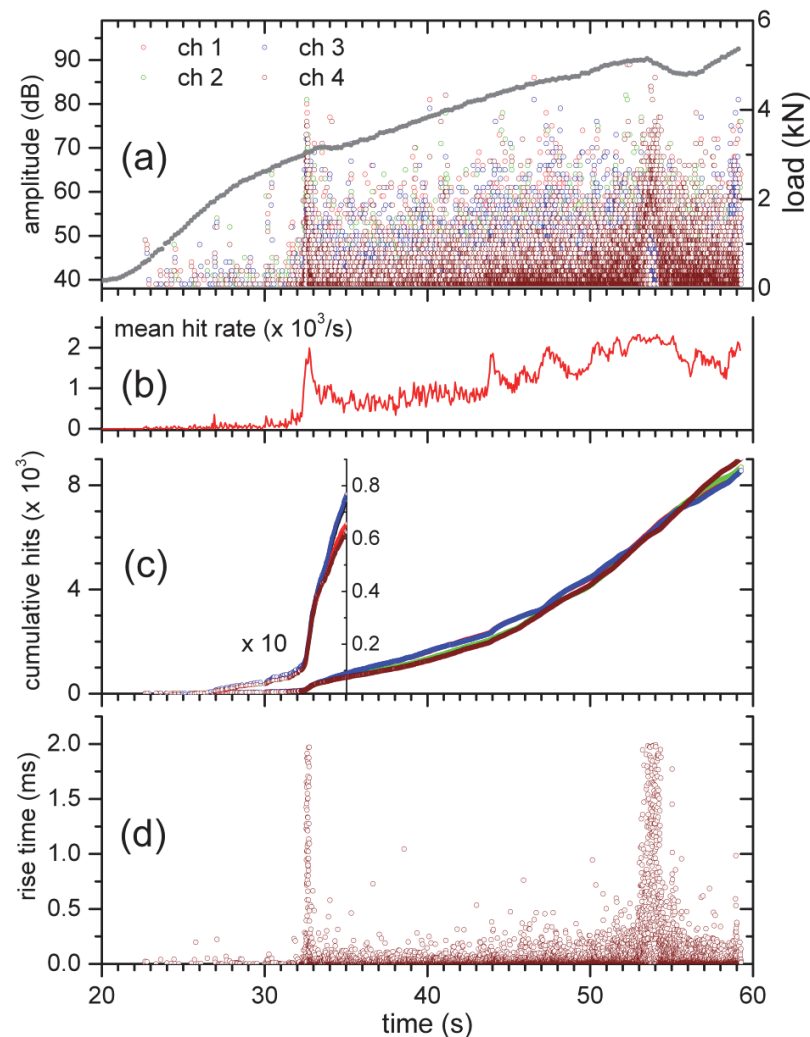
Figure 13: Time evolution of acoustic emission parameters during the CCNBD test of the specimen 2.3 (mode I fracture). (a) The distribution of amplitudes of the 4 sensors located to the front face of the specimen, in conjunction with the applied load. (b) The mean hit rate of all sensors. (c) The cumulative distribution of hits and (d) the rise time of hits recorded in channel 4.

Two-dimensional AE source localization was also conducted in order to gain additional information for the formation of the first macroscopic crack in specimens with mode I fracture.

We have to note here that the small size of the specimens as compared to the size of the sensors (5mm diameter) and the size effect to the acoustic wave velocities result to inevitable large uncertainties to the estimation of the events location, leading to the scattering of the estimated positions. However, the rejection by filtering, of the events with low amplitudes close to the threshold (Amp<44 dB) may improve the overall pattern although it reduces their total number.

A 2D location pattern derived from the signals recorded from the 4 sensors positioned at the front side of specimen 2.3 is illustrated in Fig. 14. From the first snapshot (t = 26 s) we may conclude that the AE activity initiates at the bottom tip of the chevron notch. Afterwards, events with higher amplitudes are observed to the upper tip suggesting that the stress concentration is higher in this region. However, during the formation of the macroscopic crack (t = 34 s) the events are randomly distributed around the two tips of the notch without any preferential orientation or position. Similar patterns were also estimated for the other specimens subjected to mode I fracture.

In the case of the CCNBD tests of the specimens fractured under pure mode II loading, the AE activity exhibits some similar characteristics with the mode I loading, regarding the correlation of the AE parameters with the fracture process. The AE parameters during the test of a representative specimen (specimen 3.23) are shown in Fig. 15a-d. Considerable AE activity starts at around 57% of the fracture load (5.9 kN) as it is indicated from the uniform increase of the mean hit rate in Fig. 15b. However, a small number of hits with relative high amplitudes are also recorded from the beginning of

the test, suggesting a limited formation of isolated micro-cracks. High values of RT are observed at the final stage of the rupture (after t=72 s), as in the case of the specimen 2.3, but there is no indication of any macroscopic crack before the final rupture of the specimen.
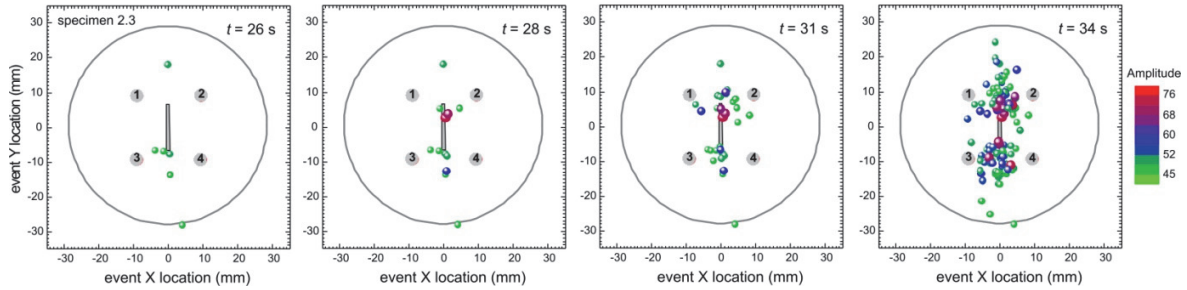

Figure 14: 2D pattern of the location of cumulative events at different selected times, during the CCNBD test of the specimen 2.3 (mode I loading). The positions of the 4 sensors at the front side of the specimen that were used in the location algorithm and the chevron notch are also indicated. The color scale denotes the highest amplitude of the recorded hits in each event and thus is an estimation of the magnitude of the events.
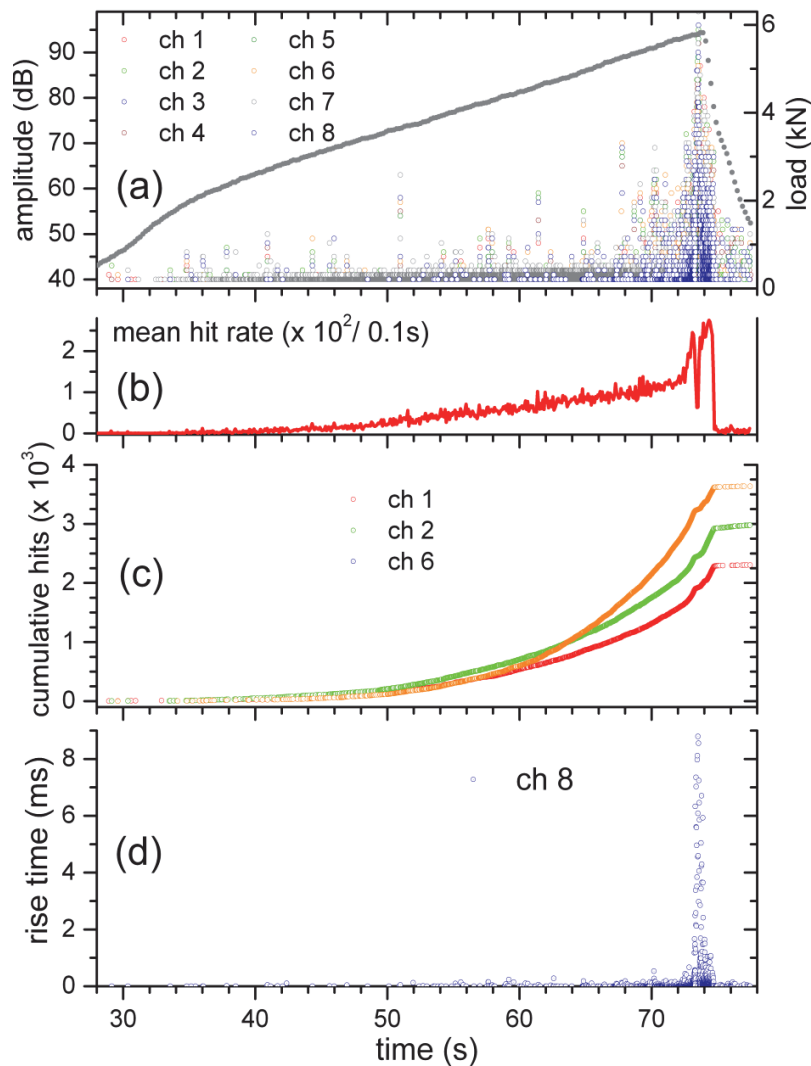

Figure 15: Time evolution of acoustic emission parameters during the CCNBD test of the specimen 3.23 (mode II fracture). (a) The distribution of amplitudes of all sensors located to the surface of the specimen, in conjunction with the applied load (b) The mean hit rate of all sensors. (c) The cumulative distribution of hits from sensors 1, 2 and 6 and (d) the rise time of hits recorded in channel 8.

Finally, a planar projection pattern of the 3D location derived from the signals recorded from all the sensors positioned at the sides of specimen 3.23 is illustrated in Fig. 16. As it is evident from the first snapshot at the early stages of the loading (t=65 s), the stress concentration should be uniform in each side of the specimen during the applied load. At the final rupture of the specimen (t=77.5 s), a rather diffused distribution of the events is observed, while their concentration at the upper tip of the chevron notch is more pronounced. The latter is consistent with the created final macroscopic crack at the upper side of the specimen (see Fig. 12). However, it should be noted that, although the location has been improved considerably by taking into account the filtered hits (Amp >46 dB) as in the case of the specimen 2.3 (Fig. 14), the discontinuity of the specimen due to the chevron notch, in conjunction with the small size of the samples, sufficiently restrict the quality of the location results.
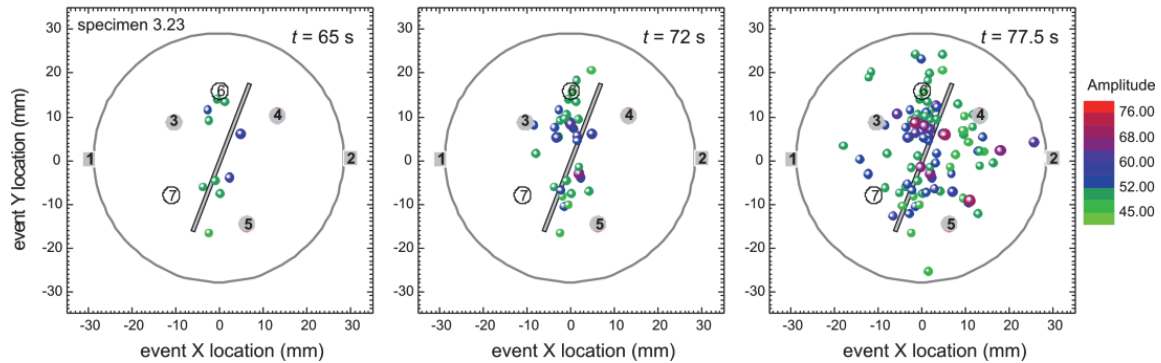

Figure 16: The projection of the 3D location of cumulative events on the circular side of the specimen 3.23 (mode II loading) at different selected times, during the CCNBD test. The positions of the sensors and the chevron notch at 23° are also indicated.

A well-established parameter that is used to determine the stages of fracture has been introduced from the field of seismology and has been modified in order to describe the amplitude distribution in AE analysis. This so-called improved b-value is defined by utilizing statistical values of the amplitude distribution, such as the mean value μ and the standard deviation σ, according to the following relation [26]:

$$I_b = \frac{log N(\mu - \alpha_1 \sigma) - log N(\mu + \alpha_2 \sigma)}{(\alpha_1 + \alpha_2)\sigma} \qquad (13)$$

where $N(\mu - \alpha_1 \sigma)$ represents the cumulative number of events with amplitudes greater than $\mu - \alpha_1 \sigma$ and $N(\mu + \alpha_2 \sigma)$ is the cumulative number of events with amplitudes greater than $\mu + \alpha_2 \sigma$. The empirical constants a_1 and a_2 are user-defined and usually take values equal to unity [26].

Low values of I_b are associated with the generation and propagation of micro-cracks and thus, the characteristic trend of its variation may serve as a qualitative index of damage in the material under investigation. In practice, a window of successive events is predetermined (usually between 50 and 100 events) and then it is shifted in order to calculate the I_b value in each window during the evolution of the experiment. The overlap between successive windows ensures the correlation of the estimated values during the time evolution of the test.

The variation of the calculated I_b values during the CCNBD tests of the specimens 2.3 (mode I loading) and 3.23 (mode II loading) are illustrated in Fig. 17 and Fig. 18, respectively. In each case, values lower than unity are associated with the formation of macroscopic cracks or/and the final failure of the specimens, as it has already been mentioned previously. Thus, in the case of the specimen 2.3, the initially observed macro-crack at around 32.5 s, as well as its final rupture at 54 s, is related with I_b values lower than 0.8 (see Fig. 17). In the case of specimen 3.23 (see Fig. 18), high values of I_b are observed up to the 90% of the failure load but after that, I_b decreases considerable reaching values below unit just before the final rupture.

Furthermore, the results obtained for mode I fracture toughness are similar to experimental results available for a different Greek marble (Dionysos marble) [27, 28, 29]. The interpretation of acoustic data for the later tests [28, 29] shows a higher damage level prior to localization.
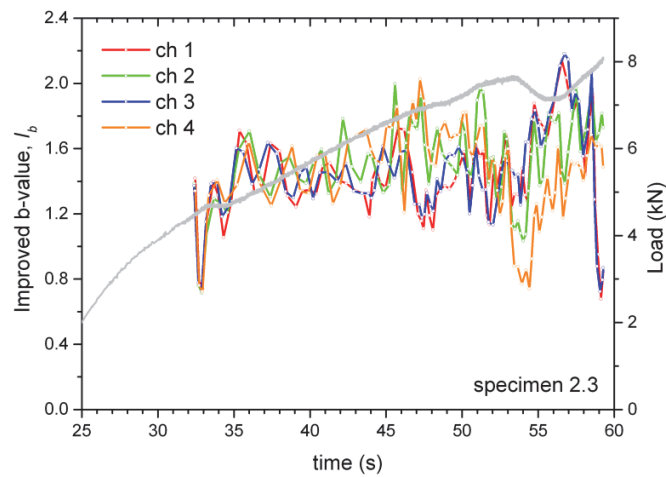
Figure 17: The variation of the improved b-value during the CCNBD test of the specimen 2.3 for each of the 4 sensors positioned in the front face (Number of successive events = 90, 50% overlapping, $a_1 = a_2 = 1$).
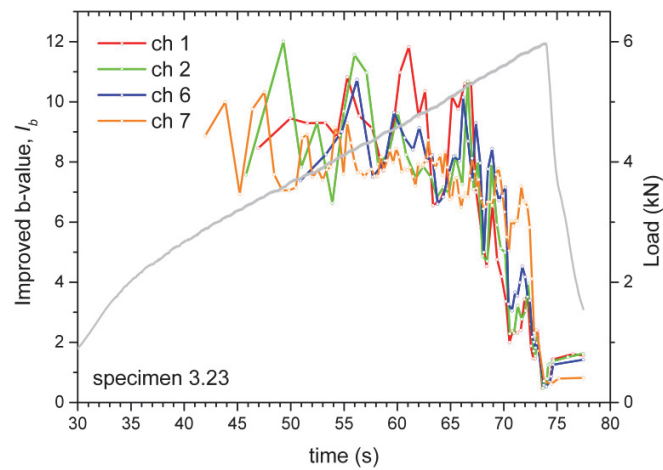

Figure 18: The variation of the improved b-value during the CCNBD test of the specimen 3.23 for 4 selected sensors (Number of successive events = 50, 50% overlapping, $a_1 = a_2 = 1$).

CONCLUSIONS

A number of CCNBD tests were carried out in order to determine the fracture toughness of Nestos marble. Specimens were also instrumented with acoustic sensors in an effort to better determine stress evolution during loading.

The available methodologies for calculating the mode I fracture toughness K_{IC} from CCNBD tests were critically evaluated and compared. In addition, the dimensional stress intensity factor of the CCNBD specimen, Y^*, is calculated with respect to the dimensionless crack length a^* using the dimensionless crack lengths (α_0 and α_1) proposed in the ISRM suggested methods [6]. The calculated minimum SIF value for the CCNBD specimen $Y^*_{min} = 1.2578$ corresponds to the critical crack length $\alpha^*_m = 0.4915$ and is comparable to published critical length values.

In addition, experimental results from the acoustic emissions monitored during the CCNBD tests are evaluated with respect to the load applied to each sample. The localization of the generated events is plotted at different time intervals during the test. Results indicate that during the early loading stages the stress concentration is uniform on both crack edges. As the load increases and the specimen is ready to fail, a rather diffused distribution of the events is observed, while their concentration at the upper tip of the chevron notch is more pronounced. Overall, using acoustic emission signals a

better determination of the failure load can be achieved, as shown in Fig 13 and 15. This failure load can then be used for the fracture toughness calculations.

Using the same experimental data, the mode I fracture toughness is calculated for each one of the different methodologies. Again, these values are comparable to each other and also correlate well with the equation proposed by Zhang [23] relating the tensile strength of rocks to their mode I fracture toughness. The mode II fracture toughness value was only calculated using the methodology proposed by Shetty et al. [5].

Future work could involve the use of an array of several sensors which will be properly positioned on the entire surface of the disc in conjunction with appropriate filtering of AE results, and an investigation of potential correlations with some of the more sophisticated analytic solutions that are available for the entire planar disc, in order to accomplish an overall analysis of the failure mechanism.

REFERENCES

[1] ISRM Testing Commission, (co-ordinator: F. Ouchterlony), Suggested methods for determining the fracture toughness of rock. Int J. Rock Mech Min Sci Geomech Abstr., 25 (1988) 71–96.

[2] Fowell, R.J., Chen, J.F., The third chevron-notch rock fracture specimen - the cracked chevron-notched Brazilian disk. Proc. 31st U.S. Symp. Rock. Balkema, Rotterdam, (1990) 295– 302.

[3] Fowell, R.J., Xu, C., The cracked chevron notched Brazilian disc test - geometrical considerations for practical rock fracture toughness measurement. Int. J. Rock Mech. Mineral Sci. Geomech. Abstr., 30 (7) (1993) 821– 824.

[4] Atkinson, C., Smelser, R.E., Sanchez, J., Combined mode fracture via the cracked Brazilian disk test. Int. J. Fract., 18 (4) (1982) 279– 291.

[5] Shetty, D.K., Rosenfiled, A.R., Duckworth, W.H., Fracture toughness of ceramics measured by a chevron notch diametral compression test. J. Am. Ceram. Soc., 68 (12) (1985) C325– C327.

[6] ISRM Testing Commission (co-ordinator: R.J. Fowell), Suggested method for determining mode I fracture toughness using cracked chevron notched Brazilian disc (CCNBD) specimens. Int J Rock Mech Min Sci Geomech Abstr., 32 (1995) 57–64.

[7] Wang, Q.Z., Jia, X.M., Kou, S.Q., Zhang, Z.X., Lindqvist, P.-A., More accurate stress intensity factor derived by finite element analysis for the ISRM suggested rock fracture toughness specimen – CCNBD. Int J Rock Mech Min Sci., 40 (2003) 233–41.

[8] Wang, Q.Z., JiaX.M., Wu L.Z., Wide-range stress intensity factors for the ISRM suggested method using CCNBD specimens for rock fracture toughness tests. Int J Rock Mech Min Sci., 41 (2004) 709–716.

[9] Wang, Q.Z., Fan H., Gou X.P., Zhang S., Recalibration and Clarification of the Formula Applied to the ISRM - Suggested for Testing Rock Fracture Toughness. Rock Mechanics and Rock Engineering, 46 (2013) 303–313.

[10] Amrollahi, H., Baghbanan, A., Hashemolhosseini, H., Measuring fracture toughness of crystalline marbles under modes I and II and mixed mode I-II loading conditions using CCNBD and HCCD specimens. Int. J. Rock Mech. Min. Sci., 48 (2011) 1123–1134.

[11] Aliha, M.R.M., Ayatollahi, M.R., Rock fracture toughness study using cracked chevron notched Brazilian disc specimen under pure modes I and II loading – A statistical approach. Theoretical and Applied Fracture Mechanics, 69 (2014) 17-25.

[12] Kaklis, K., Mavrigiannakis, S., Agioutantis Z. Bazdanis, G., An investigation of the mechanical characteristics of Nestos Marble. In: Volume in Honor of the late Professor K. Kavouridis, Technical University of Crete Publications, (2010) 57-68 (in Greek).

[13] Markides, Ch.F., Kourkoulis S.K., 'Mathematical' Cracks Versus Artificial Slits: Implications in the Determination of Fracture Toughness. Rock Mech Rock Eng., 49(3) (2016) 707–729.

[14] Chang S-H, Lee C-I, Jeon S., Measurement of rock fracture toughness under modes I and II and mixed-mode conditions by using disc-type specimens. Eng Geol., 66 (2002) 79–97.

[15] Wang, Q.Z., Stress intensity factors of the ISRM suggested CCNBD specimen used for mode-I fracture toughness determination. Int J Rock Mech Min Sci., 35 (1998) 977–982.

[16] Wang, Q.Z., Formula for calculating the critical stress intensity factor in rock fracture toughness tests using cracked chevron notched Brazilian disc (CCNBD) specimens. Int J Rock Mech Min Sci., 47 (2010) 1006–1011.

[17] Markides, C.F., Pazis D.N., Kourkoulis S.K., Stress intensity factors for the Brazilian disc with a short central crack: Opening versus closing cracks. Applied Mathematical Modelling, 35 (2011) 5636–5651.

[18] Markides, Ch.F., Kourkoulis S.K., The finite circular disc with a central elliptic hole under parabolic pressure. Acta Mechanica, 226(6) (2015) 1929–1955.

[19] Wang, Q.Z., Gou, X.P., Fan, H., The minimum dimensionless stress intensity factor and its upper bound for CCNBD fracture toughness specimen analyzed with straight through crack assumption. Engineering Fracture Mechanics, 82 (2012) 1–8.

[20] Enviroacoustics S.A., Noesis, User's manual, (2009).

[21] Agioutantis, Z., Kaklis, K., Mavrigiannakis, S., Verigakis, M., Vallianatos, F., Saltas, V., Potential of acoustic emissions from three point bending tests as rock failure precursors. Int. J. Min. Sci. Tech., 26 (2016) 155-160.

[22] Bluhm, J.I., Slice synthesis of a three-dimensional "work of fracture" specimen. Eng Fract Mech, 7 (1975) 593–604.

[23] Zhang, Z.X., An empirical relation between mode I fracture toughness and the tensile strength of rock. Int J Rock Mech Min Sci., 39 (2002) 401–406.

[24] Markides, Ch.F., Kourkoulis S.K., The circular disc under rotational moment and friction: application to the cracked Brazilian disc test. Archive of Applied Mechanics, 85(12) (2015) 1869–1897.

[25] Shiotani, T., Ohtsu, M., Ikeda, K., Detection and evaluation of AE waves due to rock deformation. Construction and Building Materials, 15 (2001) 235-246.

[26] Shiotani, T., Fujii, K., Aoki, T., Amou, K., Evaluation of progressive failure using AE sources and improved b-value on slope model tests. Progress in Acoustic Emission VII, JSNDI 7 (1994) 529-534.

[27] Dai, S. Labuz, J., Damage and failure analysis of brittle materials by acoustic emission. Journal of Materials in Civil Engineering, 9 (4) (1997) 200-205.

[28] Kaklis K., Mavrigiannakis S., Agioutantis Z., Comparison of acoustic signatures of rock specimens under uniaxial compression. ICCES'12: International Conference on Computational & Experimental Engineering and Sciences, Crete, Greece, (2012).

[29] Nomikos, P.P., Katsikogianni, P., Sakkas, K.M., Sofianos, A.I., Acoustic Emission during Flexural Loading of Two Greek Marbles. Rock Mechanics in Civil and Environmental Engineering, Zhao, Labiouse, Dudt and Mathier (eds), Taylor & Francis Group, London, (2010) 95-98.